npj | 2D materials and applications

www.nature.com/npj2dmaterials

ARTICLE OPEN

Check for updates

Raman scattering excitation in monolayers of semiconducting transition metal dichalcogenides

M. Zinkiewicz[1]✉, M. Grzeszczyk[1], T. Kazimierczuk[1], M. Bartos[2], K. Nogajewski[1], W. Pacuski[1], K. Watanabe[3], T. Taniguchi[4], A. Wysmołek[1], P. Kossacki[1], M. Potemski[1,5,6], A. Babiński[1] and M. R. Molas[1]✉

Raman scattering excitation (RSE) is an experimental technique in which the spectrum is made up by sweeping the excitation energy when the detection energy is fixed. We study the low-temperature ($T = 5$ K) RSE spectra measured on four high quality monolayers (ML) of semiconducting transition metal dichalcogenides (S-TMDs), i.e. MoS_2, $MoSe_2$, WS_2, and WSe_2, encapsulated in hexagonal BN. The outgoing resonant conditions of Raman scattering reveal an extraordinary intensity enhancement of the phonon modes, which results in extremely rich RSE spectra. The obtained spectra are composed not only of Raman-active peaks, i.e. in-plane E′ and out-of-plane A_1', but the appearance of 1st, 2nd, and higher-order phonon modes is recognized. The intensity profiles of the A_1' modes in the investigated MLs resemble the emissions due to neutral excitons measured in the corresponding PL spectra for the outgoing type of resonant Raman scattering conditions. Furthermore, for the WSe_2 ML, the A_1' mode was observed when the incoming light was in resonance with the neutral exciton line. The strength of the exciton-phonon coupling (EPC) in S-TMD MLs strongly depends on the type of their ground excitonic state, i.e. bright or dark, resulting in different shapes of the RSE spectra. Our results demonstrate that RSE spectroscopy is a powerful technique for studying EPC in S-TMD MLs.

npj 2D Materials and Applications (2024)8:2 ; https://doi.org/10.1038/s41699-023-00438-5

INTRODUCTION

The electron-phonon coupling is, in addition to the Coulomb interaction, one of the fundamental interactions between quasiparticles in solids[1]. It plays an important role in a variety of physical phenomena, in particular, low-energy electronic excitations can be strongly modified by coupling to lattice vibrations, which influences e.g. their transport[2] and thermodynamic[3] properties.

Semiconducting transition metal dichalcogenides (S-TMDs) based on molybdenum and tungsten, i.e. MoS_2, $MoSe_2$, $MoTe_2$, WS_2, and WSe_2, are the most well-known representatives of van der Waals (vdW) materials[4,5]. Their most distinguished hallmark is the transition from indirect- to direct-band gap, when thinned down from a bulk to a monolayer (ML)[6–9]. Due to the very strong absorption and direct energy band gap in the ML limit, in recent years this class of materials has become of great interest from both research[4,10–12] and development point of view[13,14]. The photoluminescence (PL) signal of S-TMDs is caused mainly by excitonic effects, even at room temperature, due to the large excitonic binding energy at the level of hundreds of meV[15–17]. It arises from the reduced dimensionality of the material and limited dielectric screening of the environment[18]. Constant progress in sample preparation, particularly the encapsulation of MLs in thin layers of hexagonal BN (hBN)[11], leads to narrowing of the observed emission lines to the limit of a few meV, which opens the possibility of studying a variety of individual excitonic complexes associated with both bright and dark states[19–37].

Raman scattering excitation (RSE) experiment performed on S-TMD MLs was proposed a few years ago in ref. [38] as a powerful technique to investigate the interaction between different excitonic complexes and phonons, i.e. exciton-phonon coupling (EPC). This approach is analogous to the PL excitation (PLE) method, in which the detected spectra are measured as a function of the excitation energy, while the detection energy/window is fixed. In the RSE experiment, the detection window can be set to cover the emission of different excitonic complexes, while the excitation energy is tuned in the energy region only slightly above (a few dozen of meV) these excitonic resonances. This results in the outgoing resonant conditions of Raman scattering (RS)[39]. The analysis of the outgoing phonon modes crossing the excitonic emission allows one to reveal the details of the exciton-phonon interaction in a given material. The RSE spectroscopy might be seen as the extension of the resonant Raman scattering method (RRS), which was extensively used to study the characteristics of phonon modes in S-TMDs[40–46]. However, a typical RRS experiment is carried out with a few selected excitation points[42–44] offering only limited access to investigate the resonant changes in the shape/intensities of the phonon modes. This restriction is lifted with the RSE measurements performed when practically continuously tuning the excitation energy[38,47,48]. RSE spectra were previously reported for bare MLs of $MoSe_2$[47] and WS_2[38] exfoliated on Si/SiO_2 substrates, as well as for the $MoSe_2$ ML encapsulated in hBN flakes[48]. In the case of the $MoSe_2$ MLs[47,48], the RSE spectrum was dominated by several phonon replicas of the LA mode. In contrast, for the WS_2 ML[38], a very rich Raman spectrum was presented with numerous phonon modes originating from the edge of the Brillouin zone (BZ) as well as multiphonon modes. Knowing that S-TMD MLs are organised into two subgroups, i.e. *bright* and *darkish*, due to the type of the ground exciton state (bright and dark, respectively)[28,32,34,49], their low-temperature

[1]Institute of Experimental Physics, Faculty of Physics, University of Warsaw, 02-093 Warsaw, Poland. [2]Central European Institute of Technology, Brno University of Technology, Brno 61200, Czech Republic. [3]Research Center for Electronic and Optical Materials, National Institute for Materials Science, 1-1 Namiki, Tsukuba 305-0044, Japan. [4]Research Center for Materials Nanoarchitectonics, National Institute for Materials Science, 1-1 Namiki, Tsukuba 305-0044, Japan. [5]Laboratoire National des Champs Magnétiques Intenses, CNRS-UGA-UPS-INSA-EMFL, 38042 Grenoble, France. [6]CENTERA Laboratories, Institute of High Pressure Physics, Polish Academy of Sciences, 01-142 Warsaw, Poland. ✉email: malgorzata.zinkiewicz@fuw.edu.pl; maciej.molas@fuw.edu.pl

($T \sim 4.2$–20 K) PL spectra display completely different complexity. The high quality of the MLs embedded between the hBN flakes, accompanied by the division of the MLs into two subgroups, has motivated us to conduct a comprehensive study devoted to the EPC in such S-TMD MLs with the aid of the RSE technique.

In this work, we use the RSE technique to investigate the exciton-phonon interaction in four high-quality samples consisting of the MoS_2, $MoSe_2$, WS_2, and WSe_2 MLs encapsulated in hBN flakes. We observe the intensity enhancements of Raman modes, while their emission energies match the emission energy of the corresponding neutral exciton (X). The measured RSE spectra are composed of many peaks that can be attributed not only from the BZ centre (Γ points) but also from other points in the BZ (e.g. M points), which are followed by lines arising from multiphonon processes. In the case of outgoing resonance conditions with the X emission, the intensity profiles of the A_1' modes in the studied MLs resemble the emission lines of the corresponding X emission. The A_1' modes' enhancements are extraordinarily strong for the WS_2 and WSe_2 MLs, but the corresponding increases of the A_1' peaks in the MoS_2 and $MoSe_2$ MLs are significantly smaller. Instead, for the Mo-based MLs, the modes involving LA phonons from the edge of the BZ, such as 2LA, 3LA, and so on, are greatly enhanced. Moreover, we observe that the A_1' intensity is also significantly enhanced when the excitation energy is in the vicinity of the X emission, which leads to the incoming resonance condition. Our experiments demonstrate that the landscape of the exciton-phonon interaction, as traced with our RSE experiments, appears to be qualitatively different in two distinct subgroups, of *bright* and *darkish*, S-TMD monolayers. The specific alignment of single-particle energy bands and the related characteristic scattering processes are speculated to account for the observed differences.

RESULTS

Raman scattering excitation spectra

Figure 1 presents false colour maps of the low-temperature ($T = 5$ K) emission intensities collected for the MoS_2, $MoSe_2$, WS_2 and WSe_2 MLs encapsulated in hBN flakes. The vertical position of a given map has been shifted to reflect the relative energy of the neutral exciton (X) emission. The assignment of the X line as arising from the neutral A exciton is straightforward and consistent with many other studies on these MLs[11,17,28,34,36]. We focus on the X lines, but we are aware that the low-temperature PL spectra of the investigated MLs are composed of several additional emission lines (see, for example, Fig. 5), particularly due to charged excitons, dark complexes, and the corresponding phonon replicas[22,23,29,31,36,50–54].

It can be seen that the line shape of the detected signal significantly depends on the excitation energy. Several parallel narrow lines superimposed on neutral exciton emissions are clearly observed in Fig. 1. These sharp lines follow the tuned excitation energy, which points out the Raman scattering as their origin and are examined in detail in the following. Moreover, for the MoS_2 and WS_2 MLs, the X emissions are strongly enhanced with decreasing excitation energies towards the respective X energies. The observed enhancement of the X intensity can be described in terms of extremely efficient formation of neutral excitons at larger *k*-vectors due to the near-resonant excitation. Note that the laser line used in experiments is narrow enough to investigate individual narrow peaks, but the excitation range of measurements is limited by the spectral range of the lasers. Moreover, the dye laser applied for MoS_2 measurements has a limited tuning accuracy. This leads to the observation of the narrow lines only at specific excitation and detection energies, in contrast to almost continuous linear evolutions present for other MLs, see Fig. 1. As is seen in the figure, the intensities of the Raman modes strongly depend on the material. For Mo-based MLs, i.e. MoS_2 and MoS_2, the intensity enhancement of different

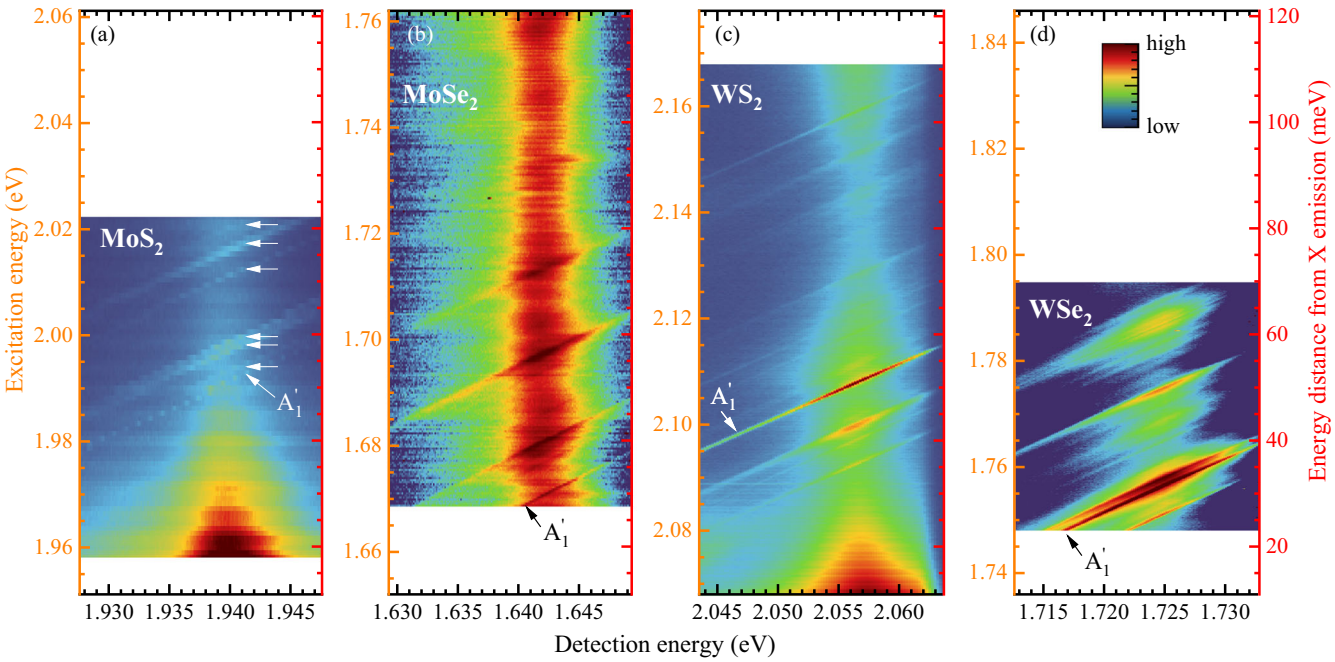

Fig. 1 Raman scattering excitation. False-colour maps of optical response of the **a** MoS_2, **b** $MoSe_2$, **c** WS_2, and **d** WSe_2 MLs encapsulated in hBN measured at low temperature ($T = 5$ K) under excitation of tuneable lasers (excitation power ~ 150 μW). The maps are vertically aligned with respect to the energy distance from the energy of the neutral exciton (X) emission in these materials, which is marked on the red right-hand energy scales. The colour scales have been normalised to the maximum intensity. The detection energies of the maps are centred around the X emission. The phonon modes are visible as several narrow parallel resonances passing diagonally across the maps. For the MoS_2 ML, white arrows point out lines which are investigated in the following.

phonon modes is similar and relatively small compared to the X intensity. In contrast, extraordinary increases in the selected Raman peaks accompanied by a large number of smaller modes are observed in the spectra measured on the WS_2 and WSe_2 MLs.

In order to investigate in detail the apparent phonon modes in the aforementioned optical responses of the MLs, the RSE spectra are plotted in Fig. 2. The RSE spectra were obtained by fixing the detection energy at the emission energy of the X line, while the excitation energy was being tuned. Note that the horizontal energy scale in the figure corresponds to the relative distance between the excitation and X energies, and is given in cm^{-1}, which is a typical unit for RS experiments and represents the so-called Raman shift. As can be seen in the inset of Fig. 2, the intensity of the A_1' modes in the W-based MLs is extraordinarily high and exceeds the X emission several times (compare with Fig. 1c and d). In contrast, the phonon modes related to the longitudinal acoustic branch, i.e. 2LA, 3LA, …, are enhanced for the Mo-based MLs, while the corresponding intensities of the A_1' modes are much smaller. All of the presented RSE spectra are very rich, consisting of many phonon modes. This confirms the resonant excitation conditions of RS, since the corresponding non-resonant Raman spectra are composed of only two Raman-active modes in the backscattering geometry of the experiment, i.e. A_1' and E′[55], whereas RS spectra become especially rich under resonant excitation conditions[40]. Using the previous results presented in the literature[38,40,43,56–58], we have identified almost all observed peaks, marked in Fig. 2 with vertical black and grey arrows. Their energies and assignments to the respective phonons are summarised in the Supporting Information (SI). Besides the two Raman-active modes from the Γ point of the BZ, the majority of the observed peaks were ascribed to phonons from the M points, which are located at the edge of the hexagonal BZ of the MLs in the middle between the K^+ and K^- points. For example, we have identified peaks related to combinations of all three branches of acoustic phonons (e.g. LA, ZA, TA) as well as their higher orders (e.g. 2LA, 3LA,…); see the SI for details. Their observation can be associated with the resonant excitation of RS, which results in the appearance of Raman inactive momentum-conserving combinations of acoustic modes from the edge of the BZ[40,59,60].

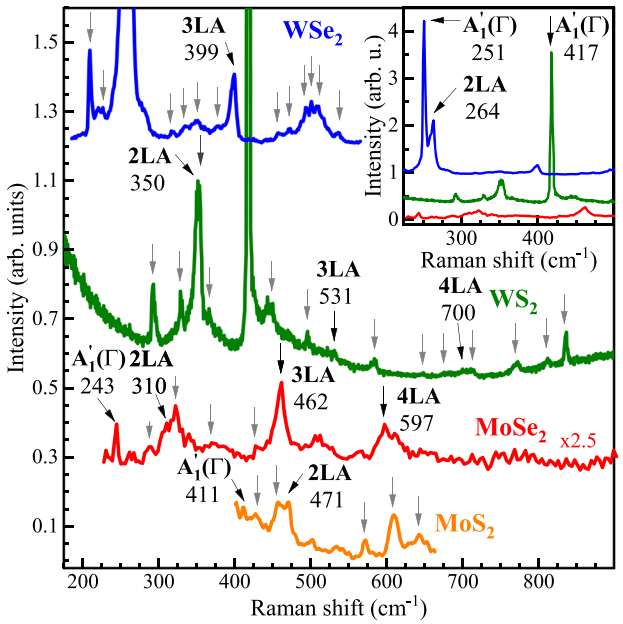

Fig. 2 RSE spectra. Raman scattering excitation (RSE) spectra detected at the energies of the X line measured on the MoS_2, $MoSe_2$, WS_2, and WSe_2 MLs encapsulated in hBN. The vertical scale has been adjusted to make the low-intensity peaks visible, while the inset shows the RSE spectra with the most pronounced peaks. Note that the RSE spectrum of the $MoSe_2$ ML was multiplied by a factor of 2.5 for clarity. The black arrows denote the labelled peaks in the Figure, while the grey arrows point to the identified peaks with their assignment presented in Supplementary Table 1 in the SI. The A_1' peaks are marked with their energy in cm^{-1}.

We have also investigated the RSE spectrum measured on the $MoSe_2$ ML grown on hBN flake using the molecular beam epitaxy (MBE) technique[61]. The ML was also covered with a thin hBN flake using mechanical exfoliation and dry transfer technique. The spectra measured for epitaxial layers exhibit peaks at energies similar to those in the case of exfoliated layers, but the relative intensity of various peaks differs. Particularly pronounced for epitaxial layers are LA replicas, which are observed from 2nd to 12th order, see SI for details.

Enhancement profiles of A_1' modes due to outgoing resonance

The resonant enhancement of the phonon modes presented above originates from the so-called outgoing resonance, which requires that the resonant excitation energy must be equal to the sum of the phonon and exciton energies[58]. To verify this hypothesis we compare the PL emissions of the X lines and the integrated intensities of the A_1' peaks in Fig. 3. The choice of A_1' modes is motivated by their substantial intensities compared to the remaining phonon modes, see Fig. 2. Note that we also

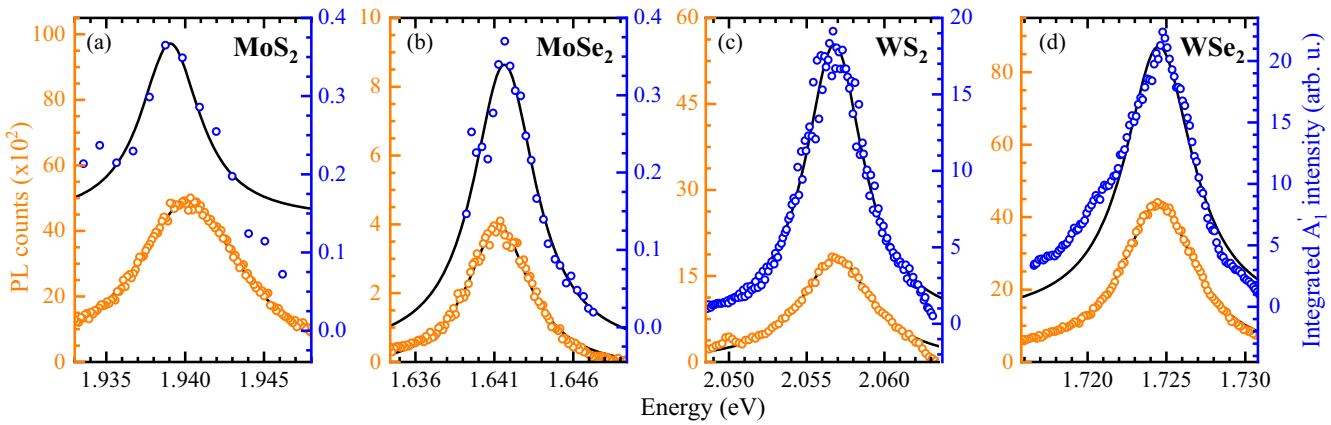

Fig. 3 PL emission versus RSE response. Comparison of (orange points) PL emissions of the X lines and (blue points) integrated intensities of the A_1' peaks measured on the **a** MoS_2, **b** $MoSe_2$, **c** WS_2, and **d** WSe_2 MLs encapsulated in hBN. Solid black curves represent the corresponding fitting using Lorentzian function.

Table 1. Summary of the obtained fitting parameters of the X emission lines and A_1' profiles using Lorentzian functions, shown in Fig. 3.

		MoS_2	$MoSe_2$	WS_2	WSe_2
X	x_c (eV)	1.940	1.641	2.057	1.727
X	w (meV)	8.3	4.9	5.7	5.5
A_1'	x_c (eV)	1.939	1.642	2.057	1.725
A_1'	w (meV)	4.6	4.8	4.5	5.3

x_c and w represent fitted energy position and the full width at half maximum (FWHM, linewidth), respectively.

analyse some other selected modes, e.g. 2ZA, 2LA, etc., in the SI, which show a similar behaviour as the one found for A_1'. As can be seen in Fig. 3, the data were fitted using Lorentzian functions, which nicely reproduce the profiles shown for both the X line and the A_1' peak. Furthermore, the parameters of the Lorentzian profiles fitted for the X lines and the A_1' peaks are summarised in Table 1. Except for the results obtained for the MoS_2 ML, the extracted profiles for the A_1' peaks, described by their energies and linewidths, follow the shape of the X emission line. For the MoS_2 ML, the observed small discrepancy in the energies of the X and A_1' peaks of about 1 meV may be explained in terms of the small energy resolution of the laser used in this case. Nevertheless, the results obtained confirm that the enhancements of the A_1' peaks in the S-TMD MLs are due to the outgoing resonance.

Outgoing versus incoming resonance

Figure 4a and b shows correspondingly a schematic illustration of the incoming and outgoing excitation resonance with the excitonic transition (X). The resonance type depends on the resonant conditions between the incident or scattered light with the X energy, while the energy difference between the excitation and the emission amounts to the phonon energy. The results presented so far are associated with the outgoing X resonance, which occurs when the scattered-photon energy is equal to that of the optical X transition. In contrast, the incoming X resonance takes place when the incident photon energy equals the energy of an optical X transition.

To study the possibility of achieving the incoming resonant conditions in S-TMD MLs, we measured the optical response of the WSe_2 ML in both the outgoing and incoming resonance conditions, see Fig. 5. The low-temperature PL spectrum of the WSe_2 ML encapsulated in hBN flakes, presented in panel (a) of the figure, displays several emission lines with a characteristic pattern similar to that previously reported in several works on WSe_2 MLs embedded in between hBN flakes[19–37]. Panel (b) and (c) display correspondingly the optical response of the WSe_2 ML in the outgoing and incoming resonances with the neutral exciton emission. As for the outgoing conditions, the observed results are analogous to those shown in Fig. 1, the incoming resonance leads to the two prominent effects. The first one, seen as a significant enhancement of all the emission lines, is associated with the resonant excitation to the X transition. Due to these conditions, the shape of the PL spectrum is strongly modified by an enormous increase in the emission intensity of the negatively charged biexciton (XX^-). The outstanding XX^- increment can be explained in terms of the considerable *n*-type doping of the studied WSe_2 ML, which results in a large reservoir of negative dark trions[21–23,36]. Due to the fact that a negatively charged biexciton is formed by a negative dark trion and a neutral bright exciton (X)[21–23,36], the resonant excitation of the X complex should cause the creation of a large population of XX^-, as is seen in Fig. 5c. The second effect is associated with the observation of several narrow peaks, parallel

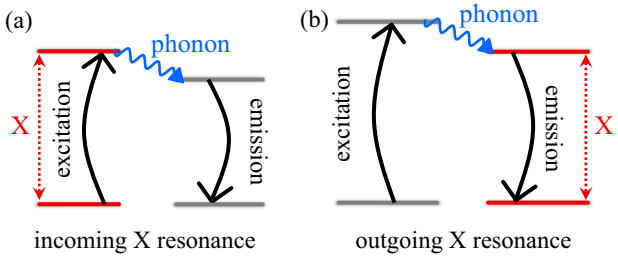

Fig. 4 Resonant Raman scattering. Schematic illustration of the **a** incoming and **b** outgoing excitation resonance with the excitonic transition, denoted as X.

to the excitation laser, which are superimposed on the enhanced emission lines below the X peak. These peaks can be ascribed to phonon modes, whose intensities are enlarged due to the incoming resonance. As in the outgoing case, the increase in the intensity depends on the phonon symmetry, resulting in the most pronounced A_1' peak.

Alike in Fig. 3, we analyse the intensity profiles of the A_1' mode measured on the WSe_2 ML under the incoming and outgoing resonance conditions of the Raman scattering with the X line, see Fig. 6. It can be seen that the A_1' evolutions can be nicely described by Lorentzian functions with similar linewidths, while their intensities differ considerably. The enhancement of the A_1' intensity is about 3 times larger in the outgoing resonance as compared to the incoming one, which can be because of several differences, such as: the strength of the exciton-phonon coupling in these two regimes, involvement of other excitonic states (e.g. dark trion or dark exciton) and of emission/absorption subprocesses, etc. For a given phonon mode, the energy separation between the outgoing and incoming resonances with a particular transition should be equal to this phonon energy. The obtained energy separation for the A_1' mode presented in Fig. 6 is of about 30 meV. This value is equivalent of 242 cm^{-1}, which is very close to the A_1' wavenumber from Fig. 2 (~251 cm^{-1}).

DISCUSSION

In the literature on the subject, a physical picture has been so far drawn that the exciton-phonon coupling in S-TMD MLs can be understood considering the symmetries of phonon modes with respect to the symmetries of orbitals associated with the involved transitions (excitons)[42]. For example, it has been established that the A_1' mode is enhanced when the excitation laser is in resonance with A and B excitons in S-TMDs, while the E′ intensity is increased under resonanant conditions matching the energy of C excitons[42,43]. Our results, shown in Fig. 2, demonstrate a substantial difference in the intensity and complexity of the RSE spectra measured on the Mo- and W-based MLs. While the A_1' modes are extraordinarily enhanced for the WS_2 and WSe_2 MLs leading to the extremely rich RSE spectra (up to 16 identified phonon modes in the WS_2 ML), the RSE spectra of the MoS_2 and $MoSe_2$ MLs are dominated by the modes involving acoustic phonons, e.g. 2LA, 3LA, …. In our opinion, this difference can be understood in terms of the excitonic states in the vicinity of their band gaps. Although S-TMD MLs share a very similar band structure, i.e. they are direct band-gap semiconductors with the minima (maxima) of the conduction (valence) band located at the K^+ and K^- points of the BZ[4,5], the arrangement of the optically active transitions in the vicinity of their band gaps is different. A strong spin-orbit coupling results in spin-split and spin-polarised subbands in both the valence band (VB) and the conduction band (CB). Consequently, MLs of S-TMD are organised into two subgroups, i.e. *bright* and *darkish*, due to the type of the ground exciton state (bright and dark, respectively)[49]. In bright MLs, the

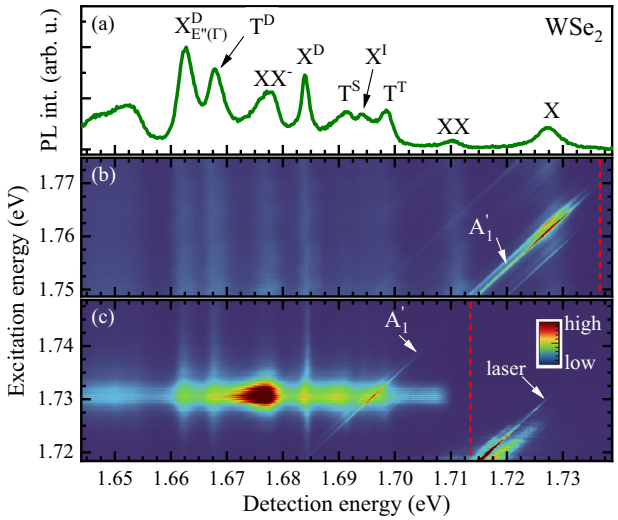

Fig. 5 Outgoing versus incoming resonant conditions. a Low-temperature ($T = 5$ K) PL spectrum of the WSe_2 ML encapsulated in hBN flakes measured using excitation energy of 2.4 eV and power of 150 μW. The lines' assignments are as follows: X—neutral exciton; XX—neutral biexciton; T^S and T^T—singlet (intravalley) and triplet (intervalley) negatively charged excitons, respectively; X^I and X^D—momentum- and spin-forbidden neutral dark excitons, respectively; XX^-—negatively charged biexciton; T^D—negatively charged dark exciton (dark trion); $X^D_{E''(\Gamma)}$—phonon replica of the X^D complex. **b**, **c** False-colour maps of low-temperature ($T = 5$ K) optical response of the WSe_2 MLs encapsulated in hBN under excitation of tuneable-energy lasers (excitation power ~ 10 μW) measured in the vicinity of the outgoing and incoming resonance conditions of Raman scattering with the X line, respectively. The colour scales in panels (**b**) and (**c**) have been normalised to the maximum intensity. The vertical red dashed lines denote the edge of the used long-pass filters.

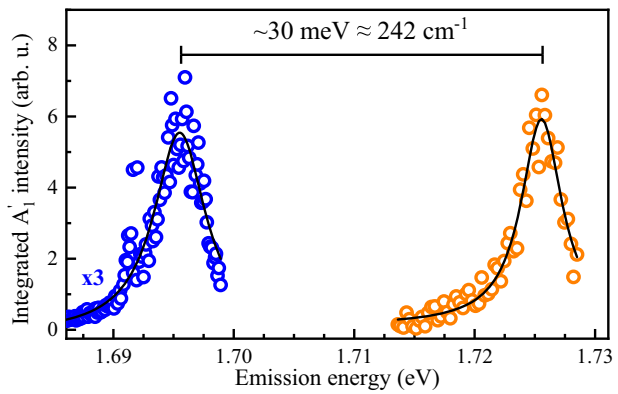

Fig. 6 RSE profiles of the A_1' mode. Intensity profiles of the A_1' mode measured on the WSe_2 ML encapsulated in hBN flakes. Blue and orange circles correspond to the incoming and outgoing resonance conditions of the Raman scattering with the X line.

excitonic recombination between the top VB and the bottom CB is optically active (bright), while the opposite happens darkish MLs. Nowadays, it is well established that for MLs encapsulated in hBN flakes, $MoSe_2$ is bright, while MoS_2, WS_2, and WSe_2 MLs are darkish (see refs. [12,28,32,34]). It means that the observed difference in the intensity of the phonon modes in the RSE spectra, shown in Fig. 2, may coincide with a particular alignment of bright and dark states in S-TMD MLs.

The substantial enhancement of the LA phonons from the M points in the $MoSe_2$ has been explained by the efficient phonon-assisted scattering occurring between the bright X exciton and the dark indirect exciton (IX) formed by an electron and a hole located at the Q and K points, respectively (see ref. [47] for details). Recently, similar description of the EPC, which occurs between the acoustic phonons from the M point and the continuum dark exciton states related to the optically forbidden transition at K and Q valleys, was demonstrated in thin layers of WS_2[62]. This confirms that for the acoustic phonons there is no significant difference between the $MoSe_2$ (bright) and WS_2 (darkish) MLs. Simultaneously, the small increase of the $A_1'(\Gamma)$ intensity in the MoS_2 ML suggests that the strength of the EPC is not remarkable. In contrast, the extraordinarily high intensity of the Raman-active $A_1'(\Gamma)$ phonon modes (does not require any additional scattering between different points in the BZ) in the W-based MLs resulting in the very rich Raman spectra can not be described using the same approach, see Fig. 2. Note that the similar difference of one order of magnitude in increment of the A_1' peaks in outgoing conditions were reported for the $MoSe_2$ and WS_2 MLs[44], which corroborate our results.

Particularly, similar results obtained for the WS_2 and WSe_2 MLs may suggest the involvement of the ground dark excitons in the efficient EPC in these materials. In the following, we speculate on the possible mechanisms, which may affect the EPC in these *darkish* materials. As the ground exciton state in W-based MLs is dark, the intensity of the bright exciton emission might be controlled by concurrent processes of the radiative recombination (emission of photons) and the relaxation process to the dark exciton and dark trion (depending on the doping level of the ML). It is known that the relative intensity of the bright and dark excitons in WSe_2 is a function of temperature[63] with a significant quenching of the X emission at low temperature. Consequently, large reservoirs of dark excitons and dark trions in W-based MLs are formed at low temperature[12,28,34], while the analogous ones will be absent in bright MLs (ground exciton state is bright). These long-lived reservoirs may increase the probability of intravalley scattering between bright excitons and dark complexes, facilitating the emission of phonons from Γ points in the WS_2 and WSe_2 MLs. It suggests that the strength of the EPC in S-TMD MLs is not only associated with the symmetries of both phonons and electronic bands[42], but may be affected by other phenomena, such as the relative order of excitonic states in the vicinity of direct transitions in K points of their BZ. The most complex are the results obtained for the MoS_2 ML, which are very similar to the ones of the $MoSe_2$ ML, i.e. the LA phonons from the M points are significantly enhanced. It is known that the MoS_2 MLs encapsulated in hBN flakes exhibit dual character. The theoretically predicted structure of the CB and VB yields optical activity of the energetically lowest transition, while including the excitonic effects leads to the dark ground excitonic state[32,50]. This may indicate that the EPC in the MoS_2 ML is more associated with its electronic band structure than with the excitonic one. The aforementioned phenomena, which may be responsible for the EPC in S-TMD MLs, requires solid theoretical analysis, which is beyond the scope of our experimental work.

Summarising, we have presented the investigation of the exciton-phonon interaction in four high-quality samples consisting of MoS_2, $MoSe_2$, WS_2, and WSe_2 MLs encapsulated in hBN flakes. By sweeping the excitation energy for a fixed value of the detection energy, we have observed an astonishing amplification of phonon-modes' intensity, while the detection energy was in resonance with neutral exciton emission. Due to this phenomenon, the measured RSE spectra are composed of many phonon modes originating not only from the BZ centre (Γ points) but also from others (e.g. M points), which are followed by lines due to multiphonon processes. For the outgoing X resonance, we have found that the intensity profiles of the A_1' modes in the studied MLs resemble the emission lines of the corresponding X emission. The A_1' enhancements are extraordinarily strong for the WS_2 and

WSe_2 MLs, but an analogous effect in the MoS_2 and $MoSe_2$ MLs are significantly smaller. For the Mo-based MLs, the modes involving acoustic phonons, such as 2LA and 3LA, are significantly enhanced. Moreover, we have observed that the A_1' intensity is also greatly strengthened since the excitation energy is in the vicinity of the X emission, leading to the incoming resonance condition. We have proposed that the difference in the obtained RSE measured on S-TMD MLs at low temperature can be understood in terms of the division of MLs into *bright* and *darkish* subgroups. These results shine new light on the exciton-phonon interaction in the MLs of S-TMDs, pointing out that not only the symmetries of phonons and excitons play an important role in this process, but also the type of their ground excitonic states.

METHODS

Sample preparation

The studied samples were composed of four S-TMD MLs, i.e. MoS_2, $MoSe_2$, WS_2 and WSe_2, encapsulated in hBN flakes and supported by a bare Si substrate. The structures were obtained by two-stage polydimethylsiloxane (PDMS)-based[64] mechanical exfoliation of bulk crystals of S-TMDs and hBN. A bottom layer of hBN in heterostructures was created in the course of non-deterministic exfoliation to achieve the highest quality. The assembly of heterostructures was realised via successive dry transfers of a ML and capping hBN flake from PDMS stamps onto the bottom hBN layer.

Experimental setup

Optical measurements were performed at low temperature ($T = 5$ K) using typical setups for the PL and PLE experiments. The investigated sample was placed on a cold finger in a continuous-flow cryostat mounted on *x*–*y* manual positioners. The non-resonant PL measurements were carried out using 514.5 nm (2.41 eV) and 532 nm (2.33 eV) radiations from the continuous wave Ar^+ and Nd:YAG lasers, respectively. To study the optical response of a ML as a function of excitation energy, i.e. to measure PLE spectra, two types of tuneable lasers were used: dye lasers based on Rhodamine 6G and DCM, and a Ti:Sapphire laser. The excitation light was focused by means of a $50\times$ long-working distance objective that produced a spot of about 1 μm diameter. The signal was collected via the same microscope objective, sent through a monochromator, and then detected by a charge-coupled device (CCD) camera. Measurements of the low-energy part of the RSE spectra, i.e. from around 15 meV from the laser line, were carried out using ultra steep edge long-pass filters mounted in front of the spectrometer.

DATA AVAILABILITY

The data that support the findings of this work are available from the corresponding authors upon reasonable request.

Received: 17 August 2023; Accepted: 11 December 2023;
Published online: 10 January 2024

REFERENCES

1. Vogl, P. in *Physics of Nonlinear Transport in Semiconductors* (NATO Science Series B) Vol. 52 (Springer New York, 1980).
2. Huewe, F. et al. Energy exchange between phononic and electronic subsystems governing the nonlinear conduction in $DCNQI_2$ Cu. *Phys. Rev. B* **92**, 155107 (2015).
3. Zhou, J. et al. Direct observation of large electron-phonon interaction effect on phonon heat transport. *Nat. Commun.* **11**, 6040 (2020).
4. Koperski, M. et al. Optical properties of atomically thin transition metal dichalcogenides: observations and puzzles. *Nanophotonics* **6**, 1289 (2017).
5. Wang, G. et al. Colloquium: Excitons in atomically thin transition metal dichalcogenides. *Rev. Mod. Phys.* **90**, 021001 (2018).
6. Mak, K. F., He, K., Shan, J. & Heinz, T. F. Control of valley polarization in monolayer MoS_2 by optical helicity. *Nat. Nanotechnol.* **7**, 494 (2012).
7. Arora, A. et al. Excitonic resonances in thin films of WSe_2: from monolayer to bulk material. *Nanoscale* **7**, 10421 (2015).
8. Arora, A., Nogajewski, K., Molas, M., Koperski, M. & Potemski, M. Exciton band structure in layered $MoSe_2$: from a monolayer to the bulk limit. *Nanoscale* **7**, 20769–20775 (2015).
9. Molas, M. R. et al. The optical response of monolayer, few-layer and bulk tungsten disulfide. *Nanoscale* **9**, 13128–13141 (2017).
10. Mak, K. F., Lee, C., Hone, J., Shan, J. & Heinz, T. F. Atomically thin MoS_2: a new direct-gap semiconductor. *Phys. Rev. Lett.* **105**, 136805 (2010).
11. Cadiz, F. et al. Excitonic linewidth approaching the homogeneous limit in MoS_2-based van der Waals heterostructures. *Phys. Rev. X* **7**, 021026 (2017).
12. Robert, C. et al. Fine structure and lifetime of dark excitons in transition metal dichalcogenide monolayers. *Phys. Rev. B* **96**, 155423 (2017).
13. Duan, X., Wang, C., Pan, A., Yu, R. & Duan, X. Two-dimensional transition metal dichalcogenides as atomically thin semiconductors: opportunities and challenges. *Chem. Soc. Rev.* **44**, 8859–8876 (2015).
14. Ye, Y. et al. Electrical generation and control of the valley carriers in a monolayer transition metal dichalcogenide. *Nat. Nanotechnol.* **11**, 598–602 (2016).
15. Stier, A. V., Wilson, N. P., Clark, G., Xu, X. & Crooker, S. A. Probing the influence of dielectric environment on excitons in monolayer WSe_2: insight from high magnetic fields. *Nano Lett.* **16**, 7054–7060 (2016).
16. Goryca, M. et al. Revealing exciton masses and dielectric properties of monolayer semiconductors with high magnetic fields. *Nat. Commun.* **10**, 4172 (2019).
17. Molas, M. R. et al. Energy spectrum of two-dimensional excitons in a nonuniform dielectric medium. *Phys. Rev. Lett.* **123**, 136801 (2019).
18. Zhu, B., Chen, X. & Cui, X. Exciton binding energy of monolayer WS_2. *Sci. Rep.* **5**, 9218 (2015).
19. Courtade, E. et al. Charged excitons in monolayer WSe_2: experiment and theory. *Phys. Rev. B* **96**, 085302 (2017).
20. Li, Z. et al. Revealing the biexciton and trion-exciton complexes in BN encapsulated WSe_2. *Nat. Commun.* **9**, 3719 (2018).
21. Chen, S.-Y., Goldstein, T., Taniguchi, T., Watanabe, K. & Yan, J. Coulomb-bound four- and five-particle intervalley states in an atomically-thin semiconductor. *Nat. Commun.* **9**, 3717 (2018).
22. Barbone, M. et al. Charge-tuneable biexciton complexes in monolayer WSe_2. *Nat. Commun.* **9**, 3721 (2018).
23. Paur, M. et al. Electroluminescence from multi-particle exciton complexes in transition metal dichalcogenide semiconductors. *Nat. Commun.* **10**, 1709 (2019).
24. Liu, E. et al. Gate tunable dark trions in monolayer WSe_2. *Phys. Rev. Lett.* **123**, 027401 (2019).
25. Li, Z. et al. Direct observation of gate-tunable dark trions in monolayer WSe_2. *Nano Lett.* **19**, 6886 (2019).
26. Li, Z. et al. Emerging photoluminescence from the dark-exciton phonon replica in monolayer WSe_2. *Nat. Commun.* **10**, 2469 (2019).
27. Li, Z. et al. Momentum-dark intervalley exciton in monolayer tungsten diselenide brightened via chiral phonon. *ACS Nano* **13**, 14107 (2019).
28. Molas, M. R. et al. Probing and manipulating valley coherence of dark excitons in monolayer WSe_2. *Phys. Rev. Lett.* **123**, 096803 (2019).
29. Liu, E. et al. Valley-selective chiral phonon replicas of dark excitons and trions in monolayer WSe_2. *Physical Review Research* **1**, 032007 (2019).
30. Liu, E. et al. Multipath optical recombination of intervalley dark excitons and trions in monolayer WSe_2. *Phys. Rev. Lett.* **124**, 196802 (2020).
31. He, M. et al. Valley phonons and exciton complexes in a monolayer semiconductor. *Nat. Commun.* **11**, 618 (2020).
32. Robert, C. et al. Measurement of the spin-forbidden dark excitons in MoS_2 and $MoSe_2$ monolayers. *Nat. Commun.* **11**, 4037 (2020).
33. Lu, Z. et al. Magnetic field mixing and splitting of bright and dark excitons in monolayer $MoSe_2$. *2D Mater.* **7**, 015017 (2019).
34. Zinkiewicz, M. et al. Neutral and charged dark excitons in monolayer WS_2. *Nanoscale* **12**, 18153–18159 (2020).
35. Robert, C. et al. Measurement of conduction and valence bands *g*-factors in a transition metal dichalcogenide monolayer. *Phys. Rev. Lett.* **126**, 067403 (2021).
36. Zinkiewicz, M. et al. Excitonic complexes in n-doped WS_2 monolayer. *Nano Lett.* **21**, 2519–2525 (2021).
37. Zinkiewicz, M. et al. The effect of dielectric environment on the brightening of neutral and charged dark excitons in WSe_2 monolayer. *Appl. Phys. Lett.* **120**, 163101 (2022).
38. Molas, M. R., Nogajewski, K., Potemski, M. & Babiński, A. Raman scattering excitation spectroscopy of monolayer WS_2. *Sci. Rep.* **7**, 5036 (2017).

39. Feng, Z. C., Perkowitz, S., Wrobel, J. M. & Dubowski, J. J. Outgoing multiphonon resonant raman scattering and luminescence near the $E_0 + \Delta_0$ gap in epitaxial CdTe films. *Phys. Rev. B* **39**, 12997–13000 (1989).
40. Gołasa, K. et al. Multiphonon resonant Raman scattering in MoS_2. *Appl. Phys. Lett.* **104**, 092106 (2014).
41. Livneh, T. & Sterer, E. Resonant Raman scattering at exciton states tuned by pressure and temperature in 2h-MoS_2. *Phys. Rev. B* **81**, 195209 (2010).
42. Carvalho, B. R., Malard, L. M., Alves, J. M., Fantini, C. & Pimenta, M. A. Symmetry-dependent exciton-phonon coupling in 2d and bulk MoS_2 observed by resonance Raman scattering. *Phys. Rev. Lett.* **114**, 136403 (2015).
43. Soubelet, P., Bruchhausen, A. E., Fainstein, A., Nogajewski, K. & Faugeras, C. Resonance effects in the Raman scattering of monolayer and few-layer $MoSe_2$. *Phys. Rev. B* **93**, 155407 (2016).
44. McDonnell, L. P., Viner, J. J. S., Rivera, P., Xu, X. & Smith, D. C. Observation of intravalley phonon scattering of 2s excitons in $MoSe_2$ and WSe_2 monolayers. *2D Mater.* **7**, 045008 (2020).
45. Kumar, D., Singh, B., Kumar, R., Kumar, M. & Kumar, P. Davydov splitting, resonance effect and phonon dynamics in chemical vapor deposition grown layered MoS_2. *Nanotechnology* **32**, 285705 (2021).
46. Klein, J. et al. Electrical control of orbital and vibrational interlayer coupling in bi- and trilayer 2H-MoS_2. *Phys. Rev. Mater.* **6**, 024002 (2022).
47. Chow, C. M. et al. Phonon-assisted oscillatory exciton dynamics in monolayer $MoSe_2$. *npj 2D Mater. Appl.* **1**, 33 (2017).
48. Shree, S. et al. Observation of exciton-phonon coupling in $MoSe_2$. *Phys. Rev. B* **98**, 035302 (2018).
49. Molas, M. R. et al. Brightening of dark excitons in monolayers of semiconducting transition metal dichalcogenides. *2D Mater.* **4**, 021003 (2017).
50. Grzeszczyk, M. et al. Exposing the trion's fine structure by controlling the carrier concentration in hBN-encapsulated MoS_2. *Nanoscale* **13**, 18726–18733 (2021).
51. Klein, J. et al. Trions in mos_2 are quantum superpositions of intra- and intervalley spin states. *Phys. Rev. B* **105**, L041302 (2022).
52. Park, S. et al. Efficient valley polarization of charged excitons and resident carriers in molybdenum disulfide monolayers by optical pumping. *Commun. Phys.* **5**, 73 (2022).
53. Smoleński, T. et al. Interaction-induced Shubnikov–de Haas oscillations in optical conductivity of monolayer $MoSe_2$. *Phys. Rev. Lett.* **123**, 097403 (2019).
54. Rodek, A. et al. Controlled coherent-coupling and dynamics of exciton complexes in a $MoSe_2$ monolayer. *2D Mater.* **10**, 025027 (2023).
55. Zhang, X. et al. Phonon and Raman scattering of two-dimensional transition metal dichalcogenides from monolayer, multilayer to bulk material. *Chem. Soc. Rev.* **44**, 2757–2785 (2015).
56. Shi, W. et al. Raman and photoluminescence spectra of two-dimensional nanocrystallites of monolayer WS_2. *2D Mater.* **3**, 025016 (2016).
57. Carvalho, B. R. et al. Intervalley scattering by acoustic phonons in two-dimensional MoS_2 revealed by double-resonance Raman spectroscopy. *Nat. Commun.* **8**, 14670 (2017).
58. Zinkiewicz, M. et al. Emission excitation spectroscopy in WS_2 monolayer encapsulated in hexagonal BN. *Acta Phys. Pol. A* **136**, 624–627 (2019).
59. Molas, M. R. et al. Tuning carrier concentration in a superacid treated MoS_2 monolayer. *Sci. Rep.* **9**, 1989 (2019).
60. Bhatnagar, M. et al. Temperature induced modulation of resonant Raman scattering in bilayer 2H-MoS_2. *Sci. Rep.* **12**, 14169 (2022).
61. Pacuski, W. et al. Narrow excitonic lines and large-scale homogeneity of transition-metal dichalcogenide monolayers grown by molecular beam epitaxy on hexagonal boron nitride. *Nano Lett.* **20**, 3058–3066 (2020).
62. Tan, Q.-H. et al. Quantum interference between dark-excitons and zone-edged acoustic phonons in few-layer WS_2. *Nat. Commun.* **14**, 88 (2023).
63. Zhang, X.-X., You, Y., Zhao, S. Y. F. & Heinz, T. F. Experimental evidence for dark excitons in monolayer WSe_2. *Phys. Rev. Lett.* **115**, 257403 (2015).
64. Castellanos-Gomez, A. et al. Deterministic transfer of two-dimensional materials by all-dry viscoelastic stamping. *2D Mater.* **1**, 011002 (2014).

ACKNOWLEDGEMENTS

The work was supported by the National Science Centre, Poland (grants no. 2017/27/B/ST3/00205, 2018/31/B/ST3/02111, and 2021/41/B/ST3/04183), EU Graphene Flagship Project, and the CNRS via IRP "2DM" project. M.B. acknowledges support from the Grant Agency of the Czech Republic under grant no. 23-05578S. K.W. and T.T. acknowledge support from the JSPS KAKENHI (Grant Numbers 21H05233 and 23H02052) and World Premier International Research Center Initiative (WPI), MEXT, Japan. M.P. acknowledges the support from the Foundation for Polish Science (MAB/2018/9 Grant within the IRA Program financed by EU within SG OP Program).

AUTHOR CONTRIBUTIONS

M.Z., M.G., T.K., A.W., P.K., M.P., A.B. and M.R.M. performed the experiments. K.N. and M.B. fabricated the samples with exfoliated monolayers. W.P. grew the sample with an epitaxial $MoSe_2$ monolayer K.W. and T.T. grew the hBN crystals. M.R.M. initiated and supervised the project. M.Z. and M.R.M. wrote the manuscript with inputs from all co-authors.

COMPETING INTERESTS

The authors declare no competing interests.

ADDITIONAL INFORMATION

Supplementary information The online version contains supplementary material available at https://doi.org/10.1038/s41699-023-00438-5.

Correspondence and requests for materials should be addressed to M. Zinkiewicz or M. R. Molas.

Reprints and permission information is available at http://www.nature.com/reprints

Publisher's note Springer Nature remains neutral with regard to jurisdictional claims in published maps and institutional affiliations.